The structure and spectrum of the anisotropically confined two-dimensional Yukawa system

1998 J. Phys.: Condens. Matter 10 11627

(http://iopscience.iop.org/0953-8984/10/50/004)

J. Phys.: Condens. Matter **10** (1998) 11627–11644. Printed in the UK PII: S0953-8984(98)95442-X

The structure and spectrum of the anisotropically confined two-dimensional Yukawa system

Ladir Cândido†, José-Pedro Rino†, Nelson Studart† and François M Peeters‡

† Departamento de Física, Universidade Federal de São Carlos, São Carlos, São Paulo, 13565-905, Brazil

‡ Departement Natuurkunde, Universiteit Antwerpen (UIA), Universiteitsplein 1, B-2610 Antwerpen, Belgium

Received 29 June 1998, in final form 4 September 1998

Abstract. We have studied the structural and spectral properties of the classical system consisting of a finite number of charged particles, moving in two dimensions (2D), and interacting through a screened Coulomb potential and held together by an anisotropic harmonic potential. It is known that for the bare Coulomb interaction, the system crystallizes in well defined ordered configurations in which the particles are distributed in shells. However, we have found that the occupation of the shells changes considerably as a function of the screening parameter, and for large screening, the shell structure disappears and the particles form a Wigner lattice. We have shown that the eigenmodes of the system stiffen with increasing screening. By increasing the anisotropy of the confining potential, we were able to drive the system from 2D to 1D; this change occurs through a series of structural transitions. These transitions are reflected in the mode spectrum which collapses into a narrower frequency region with increasing anisotropy.

1. Introduction

There has recently been growing interest in studying clusters of a finite number of interacting particles subjected to an external confinement potential. Electrons confined in semiconductor quantum dots [1], plasmas of electrons and ions in radio-frequency traps [2], a high density of a cold ionic system in storage rings [3], electrons or ions trapped near the superfluid helium interfaces [4], strongly coupled dusty plasmas [5], and polymer colloids confined between glass plates [6] are examples of different trap configurations. For charged particles and isotropic parabolic confinement, the model describing the system is similar to the Thomson classical model of an atom [7]. A shell structure is obtained and it is possible to build up a Mendeleev table for both two- and three-dimensional atoms [8, 9]. Order–disorder transitions for phases corresponding to inter-shell rotation and inter-shell diffusion in two-dimensional (2D) charged systems were found and the excitation spectrum was evaluated [10]. These studies were recently extended to analyse configurations of artificial molecules formed by double-layer atoms [11].

Most of the previous studies have been performed by considering the bare Coulomb interaction among the particles. However, the 2D Yukawa system has been used as a simple model for charged colloidal suspensions [12, 13]. On the other hand, in the case of anisotropic 3D confinement, which usually occurs in traps, novel configurations and different structural phase transitions can be found as a function of the number of particles as well as the anisotropy of the confining potential [14].

0953-8984/98/5011627+18$19.50

In this paper, we consider a cluster of classical particles, moving in 2D, and interacting with each other through the Yukawa potential and subject to an anisotropic parabolic potential. The purpose of the present investigation is to analyse in detail the shape and internal structure of the clusters and how changes in these configurations occur as both the screening parameter of the Yukawa interaction potential and the anisotropy parameter of the confinement potential are varied.

The paper is organized as follows. In section 2 we describe the model and our numerical approach. In section 3 the structural and dynamical properties of the system are discussed. We analyse how the stable-state configurations, vibrational density of states, and the excitation spectrum are influenced by the screening. We observe a new structural transition, for a fixed number of particles, from a shell structure at small values of the screening constant to a Wigner lattice-like cluster for strong screening. In section 4 we discuss the influence of the anisotropy of the confinement potential on the stable-state configurations and the normal-mode excitation spectrum of Coulomb clusters. Different structural phase transitions are found with increasing anisotropy. Finally, in section 5 we present the role of the screening potential in the structural transitions induced by the anisotropy of the confinement potential, and we summarize our results and present our conclusions. We think that the experiments on dusty plasmas [5] and colloidal particles [6] are good candidates as regards seeing the effects that we predict in this work. In these systems, the plasma of charged particles adjusts self-consistently to provide shielding, and can be modelled by a screened Coulomb potential.

2. The model and the numerical approach

Our model consists of a 2D classical system consisting of a finite number (N) of particles with identical charge (Ze) moving in a medium with dielectric constant ϵ and interacting through a repulsive screened Coulomb (i.e. Yukawa) inter-particle potential. A confinement potential keeps the particles together; it is taken to be harmonic. The potential energy of the system is given by

$$V = \sum_{i=1}^{N} \frac{1}{2} m {\omega_0}^2 ({x_i}^2 + \alpha {y_i}^2) + \frac{(Ze)^2}{\epsilon} \sum_{j>i=1}^{N} \frac{\exp(-|\boldsymbol{r}_i - \boldsymbol{r}_j|/\lambda)}{|\boldsymbol{r}_i - \boldsymbol{r}_j|} \tag{1}$$

where m is the mass of the particles with position coordinates $\boldsymbol{r}_i = (x_i, y_i)$, ω_0 the strength of the confinement potential which, for generality, is taken anisotropic with anisotropy parameter α, and λ is the screening length, which we assume to be constant. Hence, it is more a measure of the range of the potential than a genuine screening length. In order to make clear the effective number of parameters that the system depends on, we introduce the following dimensionless units [8]: $r_0 = (Z^2 e^2/\epsilon\gamma)^{1/3}$ for the unit of length where $\gamma = m{\omega^2}_0/2$, $E_0 = \gamma r_0^2$ for the unit of energy, and $\tau = \sqrt{2}/\omega_0$ as the unit of time. The dimensionless potential energy becomes

$$V = \sum_{i=1}^{N} ({x_i}^2 + \alpha {y_i}^2) + \sum_{j>i=1}^{N} \frac{\exp(-\kappa|\boldsymbol{r}_i - \boldsymbol{r}_j|)}{|\boldsymbol{r}_i - \boldsymbol{r}_j|} \tag{2}$$

where $\kappa = r_0/\lambda$ is the dimensionless inverse screening length, which is a measure of the range of the inter-particle interaction. Note that the stable-state configuration will depend on the following three parameters: (1) N: the number of particles; (2) α: the anisotropy of the confinement potential; and (3) κ: the inverse screening length. In references [8, 9], the parameter space $(N, \alpha, \kappa) = (N, 1, 0)$ was studied, which is the region of classical

Coulomb clusters in a symmetric parabolic confinement potential. Here we extend these previous studies to the full (N, α, κ) parameter region.

In order to find the stable-state configuration of the system and to study the dynamics, we have used the technique of molecular dynamics (MD) simulation. The MD simulations were carried out using the procedure outlined by Hasse and Schiffer [15]. We started with a random distribution of particles at high temperature, around $T_0 = E_0/k_B$, and followed the time evolution with time steps in the range $\Delta t = (0.005\text{–}0.01)\tau$ depending on N and κ. Afterwards, the system was cooled down by successively decreasing the temperature by 20% after each 50 Δt until the temperature reached $T \sim 10^{-20}T_0$. In order to obtain the stable state of the system, different initial distributions were taken in order to ascertain that the stable state was reached. The physical quantities are obtained by averaging over 5×10^4 Δt after the system was thermalized, which was taken to have occurred after a time $t = 10^5$ Δt.

3. The dependence on the screening

In this section, we limit ourselves to considering an isotropic confinement potential, i.e. with $\alpha = 1$, and investigate the stable-state configuration as function of the screening constant κ and the number of particles N in the cluster. First we consider the stable-state configuration and the respective energy. Next, the spectrum, i.e. the normal modes, and the velocity correlation function are investigated.

3.1. The structure of the minimum-energy configurations

In the absence of screening, i.e. for $\kappa = 0$, previous studies [8, 16, 9] have shown that the particles arrange themselves in rings (also called shells). The number of particles on each ring and the number of rings depend on N and were catalogued into a Mendeleev type of table [8, 9]. For small values of κ we still recover this ring structure; the population of each ring can be a function of κ, but for sufficiently large screening the particles arrange themselves into a finite triangular Wigner crystal.

This behaviour is illustrated in figure 1 for $N = 30$ particles and for different values of κ. For clarity we added circles in order to accentuate the shell structure. Note that each shell has a finite width and the radial positions in each of the rings are not exactly the same. Notice that for $\kappa = 0$ we recover the $(5, 10, 15)$ configuration as had already been discovered in reference [8] for a Coulomb system. On increasing the screening, we find that for $\kappa = 1$ the shell structure $(5, 11, 14)$ becomes the stable state, and for $\kappa = 5$ it becomes $(1, 6, 11, 12)$. On increasing the screening beyond $\kappa = 5$, the system transforms into a Wigner lattice. For very large κ, the screened interaction becomes extremely short ranged, and the particles 'prefer' to locate near $r \approx 0$, where the confinement vanishes, and, as a result, the system becomes similar to the 2D Wigner solid with hexagonal symmetry. Notice that recently [8, 9, 17] it was shown that the functional form of the circular confinement potential may also influence the shell structure, i.e. the detailed distribution of the particles over the different rings.

The difference between these different states can be made more quantitative by considering the bond-angle distribution $f(\theta)$, which is plotted in figure 2 for the previous system with $N = 30$. The bond-angle distribution is obtained from our MD simulation as follows: first a list of all i nearest-neighbour electrons around a fixed electron O is constructed using a cut-off distance which is given by the position of the first minimum in $g_{iO}(r)$. From this list, the angles $\angle\, i\text{–}O\text{–}i$ are calculated for all i nearest-neighbour

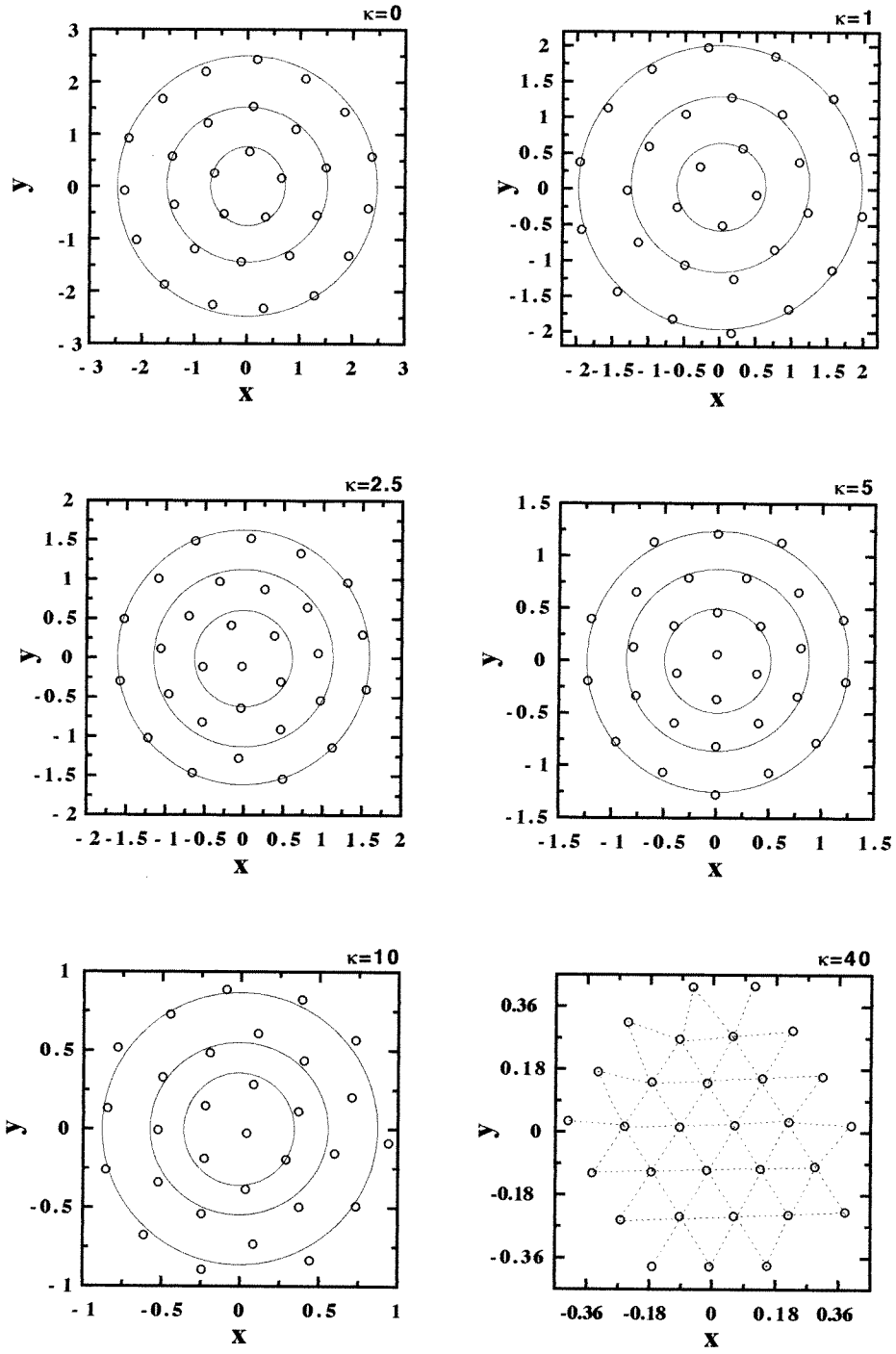

Figure 1. Evolution of the minimum stable configuration for the cluster of $N = 30$ particles for different values of the screening parameter $\kappa = 0$, 1, 2.5, 5, 10, 40. Note that the x- and y-scales shrink as κ increases.

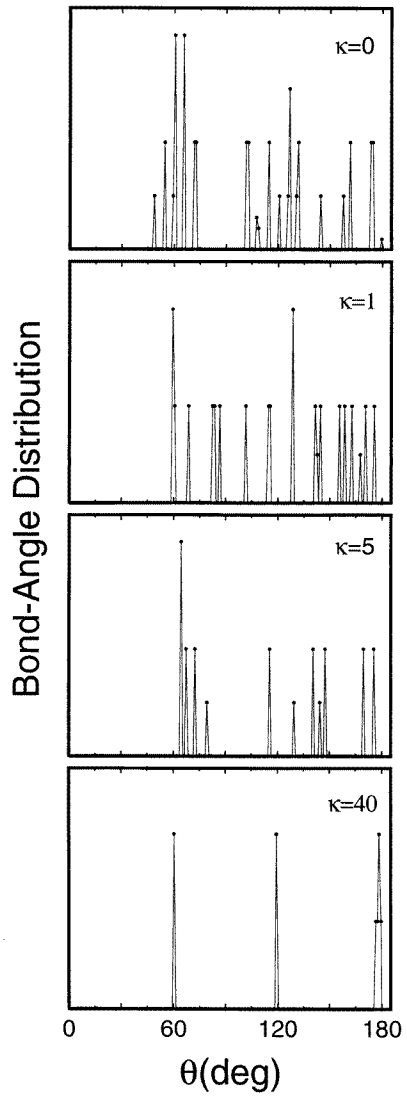

Figure 2. The distribution of the bond angles for $N = 30$ particles and $\kappa = 0$, 1, 5, 40.

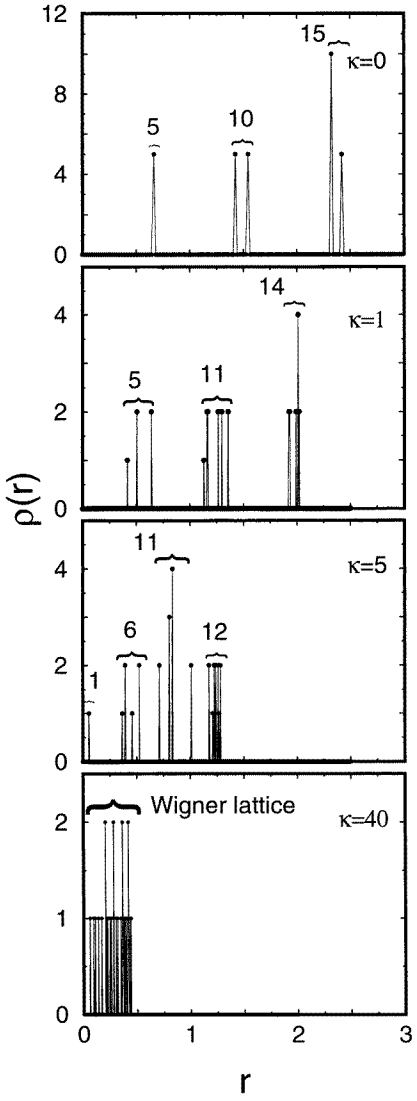

Figure 3. The radial distribution for a system consisting of $N = 30$ particles for $\kappa = 0$, 1, 5, 40.

electrons. The histogram in figure 2 is then made up of averages over all angles obtained involving all electrons at position O in the stable-state configuration. We clearly see that with increasing κ the bond angles start to group increasingly near 60, and integer multiples of it, indicating an increased tendency towards forming a triangular Wigner lattice.

The ring structure is more clearly investigated by considering the radial distribution function, which is shown in figure 3 for the $N = 30$ system. After the system was thermalized, the time evolution of the radial positions of the particles was followed over a time interval 5000 Δt from which we obtain a time-averaged radial distribution function $\rho(r)$ at $T = 10^{-20}T_0$. From figure 3, we clearly observe the changes in the electron density in the different rings as a function of κ, which is a consequence of the redistribution of the

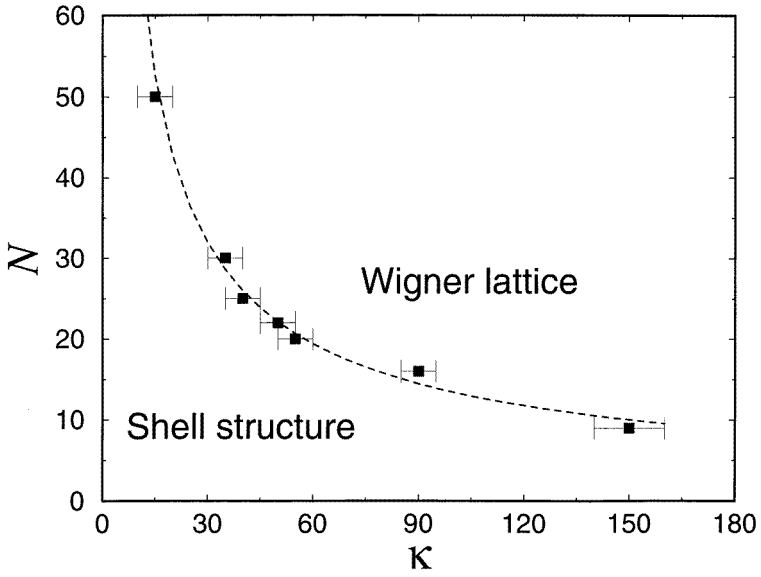

Figure 4. The (N, κ) phase diagram.

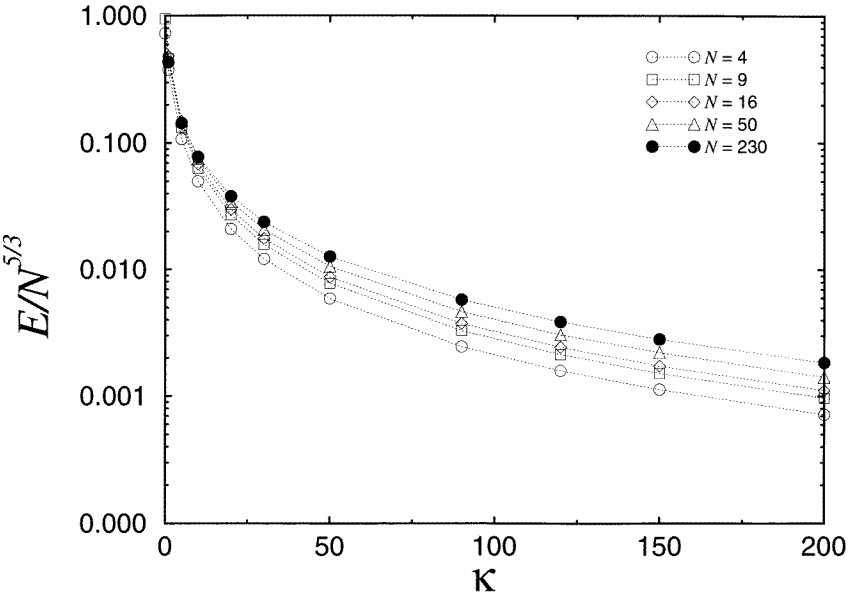

Figure 5. The screening constant dependence of the minimum energy of the stable state scaled with respect to $N^{5/3}$ for different cluster sizes.

particles over different rings with increasing κ. Notice that, on increasing κ, the system becomes increasingly dense due to the decreasing repulsion between the particles.

The transition of the system from the shell structure to the Wigner lattice is summarized in the phase diagram shown in figure 4. The phase diagram is determined from a direct analysis of $\rho(r)$ and $f(\theta)$. The numerical results are indicated by the symbols and the dashed

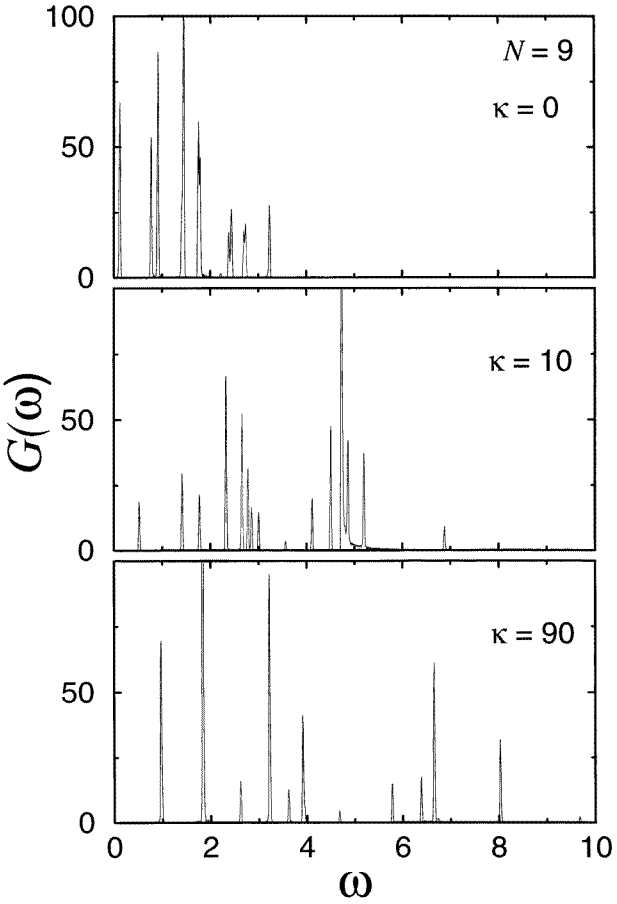

Figure 6. The vibrational density of states $G(\omega)$ for $\kappa = 0$, 10, 90, and $T = 10^{-7}T_0$, for a cluster with $N = 9$ particles.

line is the function $N = 370\,\kappa^{-0.72}$ which was obtained through a fit of our numerical results. The error bars in figure 4 are an indication that the transition is not abrupt, but occurs over a finite width. Note that, with increasing N, the lattice state is reached for smaller values of the screening constant. This is not surprising because for large N-values it was already found [8] that, for a Coulomb system of particles, the inner part of the cluster is arranged into a Wigner lattice and the shell structure is only found near the edge of the cluster. Thus, on increasing N, a larger part of the particles in the cluster are already arranged into a Wigner lattice configuration and consequently it requires only a much smaller softening of the inter-particle potential in order to induce the transition of the total system into the Wigner lattice state.

3.2. The minimum energy of the equilibrium state

The lowest energy of the stable state as a function of the screening parameter κ is shown in figure 5. For the Coulomb system it has been shown [18] that for large N the energy behaves like $E \sim N^{5/3}$. So, we show the dependence of the stable-state energy, scaled with respect

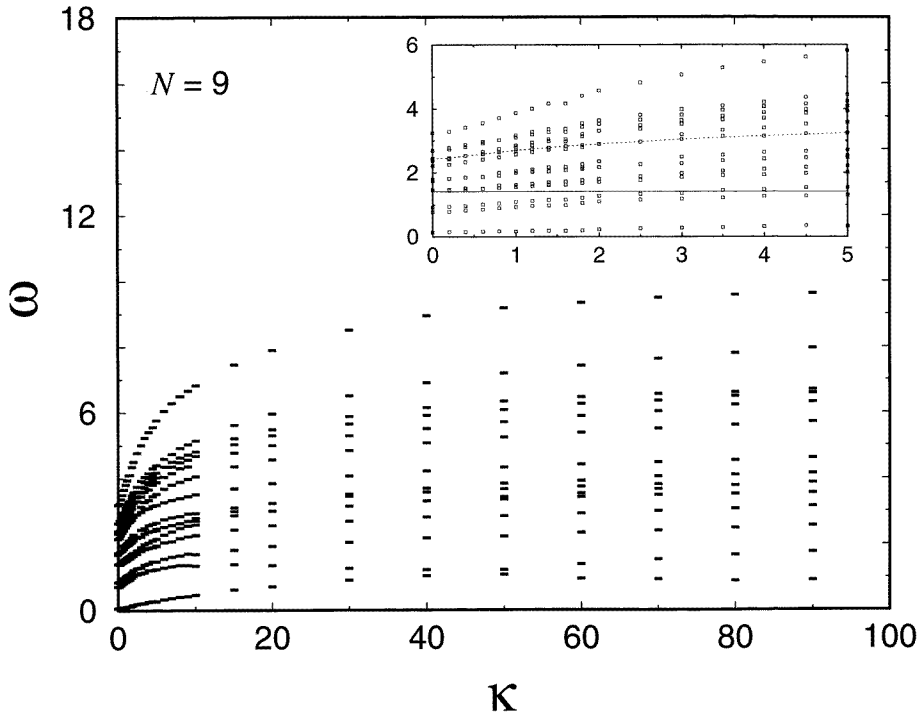

Figure 7. The excitation spectrum as a function of κ corresponding to the peaks of $G(\omega)$ for $N = 9$ and $T = 10^{-7}T_0$. The inset shows the small-κ region where the solid line gives the frequency for the centre-of-mass motion and the dashed curve is the breathing mode.

to $N^{5/3}$, on the screening parameter κ for several cluster sizes. We clearly observe that our results reproduce the general power law in the case of pure Coulomb interaction but that this is less so for increasing κ. Note also that the equilibrium-state energy decreases with increasing screening which is a consequence of the decreasing range of the inter-particle interaction.

3.3. Dynamical properties

From the MD simulation, we obtain the time evolution of the position and the velocity of the different particles in the system from which we can calculate the different correlation functions. Here, we will concentrate on the velocity–velocity correlation function and investigate its dependence on the screening parameter. The normalized velocity auto-correlation function is defined as follows:

$$Z(t) = \frac{\langle \boldsymbol{v}_i(t) \cdot \boldsymbol{v}_i(0) \rangle}{\langle \boldsymbol{v}_i(0) \rangle^2} \tag{3}$$

where $\boldsymbol{v}_i(t)$ is the velocity of the particle i at time t, and the average $\langle \cdots \rangle$ denotes an *equilibrium* ensemble average over the particles. The Fourier transform of this function

$$G(\omega) = \int_0^\infty \mathrm{d}t \ \mathrm{e}^{\mathrm{i}\omega t} Z(t) \tag{4}$$

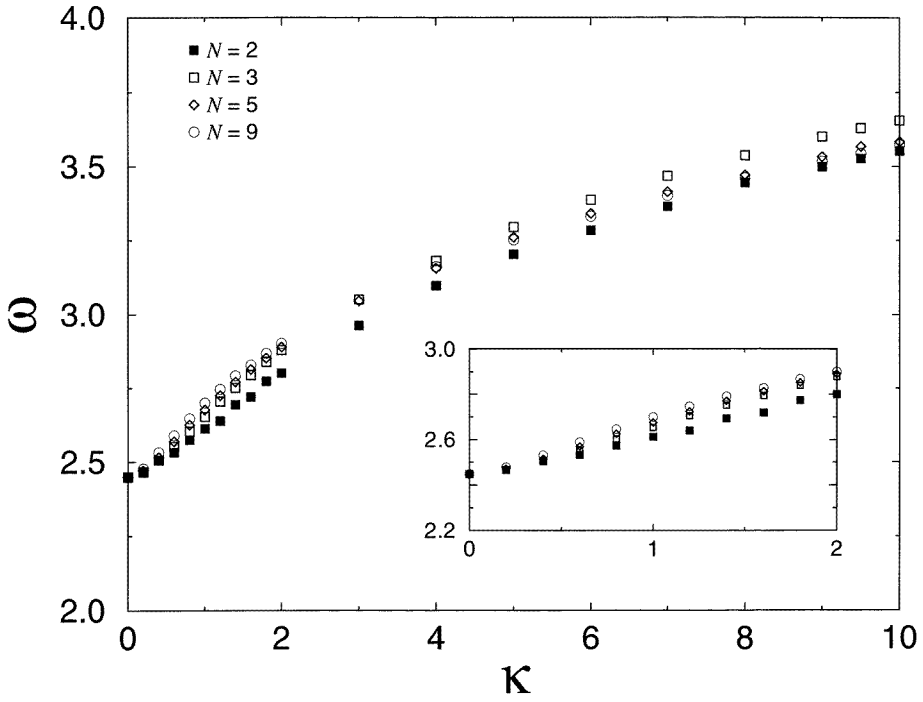

Figure 8. The frequency of the breathing mode as a function of κ for small-size clusters with $N = 2, 3, 5, 9$. The inset enlarges the small-κ region.

reflects the vibrational density of states of the system and consequently the normal-mode frequencies, or equivalently the energy spectrum [20].

In figure 6, the Fourier transform of the velocity auto-correlation function is shown for a system consisting of $N = 9$ particles around zero temperature (we took $T = 10^{-7}T_0$) and for three values of the screening parameter: $\kappa = 0, 10, 90$. The $\kappa = 0$ result agrees with the one found in reference [20] where the dynamics of a finite system of interacting Coulomb particles was investigated. The motion of particles was considered with respect to the centre-of-mass motion and consequently the mode with frequency $\omega = \omega_0$ does not appear in the velocity auto-correlation function. Notice that with increasing screening the peaks in the spectrum are shifted to larger frequencies, i.e. the system becomes stiffer. This behaviour is summarized in figure 7, where we show the position of the different peaks in $G(\omega)$ as a function of the screening parameter κ for $N = 9$. There is a monotonic increase of the different frequencies with κ. In the inset of figure 7, we show the small-κ behaviour, from which we notice that the different eigenfrequencies exhibit a linear increase with κ. This behaviour can be understood from the functional behaviour of the inter-particle interaction. The squares of the eigenfrequencies are, in essence, determined by the second derivative of the inter-particle potential

$$V''(r) = (2 + 2\kappa r + (\kappa r)^3)(\mathrm{e}^{-\kappa r}/r^3).$$

When we approximate the inter-particle distance by its average value $\langle r \rangle$, we expect that, in a crude approximation, the κ-functional behaviour of the eigenfrequencies should be given by $\omega \approx [V''(\langle r \rangle)]^{1/2}$. The average nearest-neighbour inter-particle distance $\langle r \rangle$ was

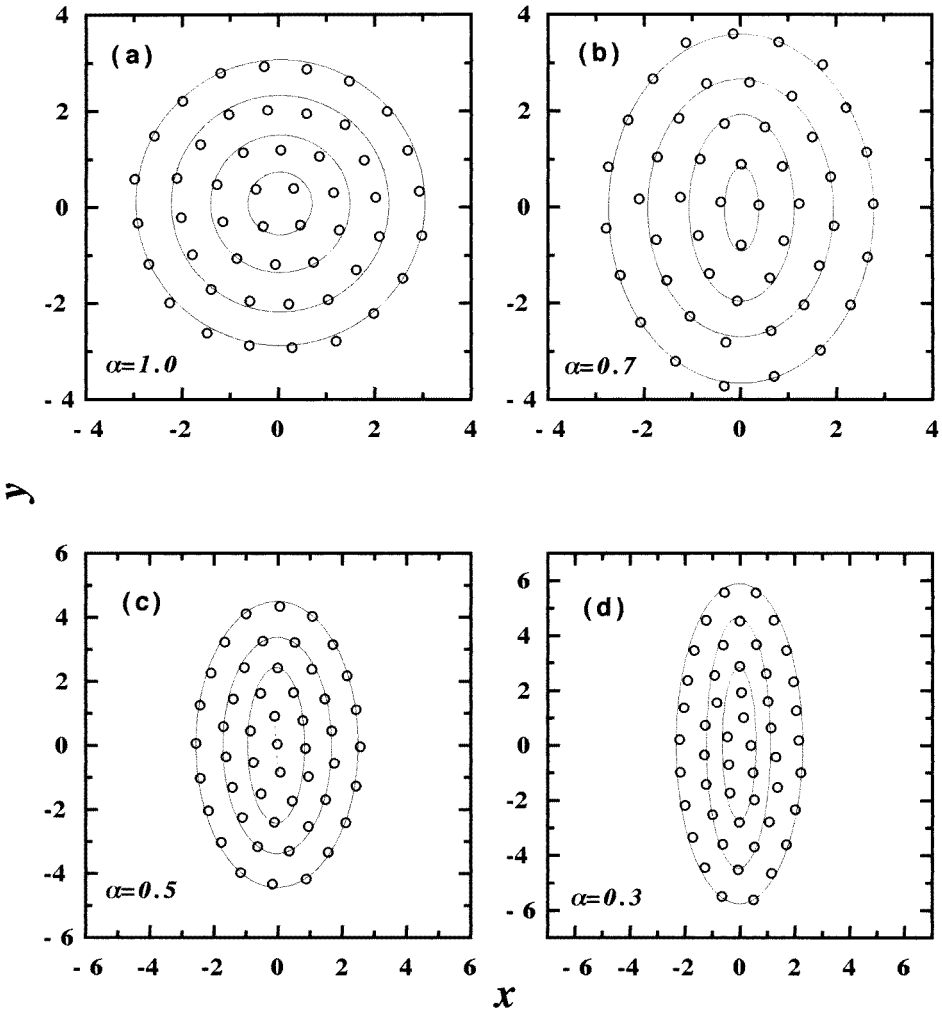

Figure 9. The configuration of the $N = 50$ cluster for different values of the anisotropy parameter: (a) $\alpha = 1$, (b) $\alpha = 0.7$, (c) $\alpha = 0.5$, (d) $\alpha = 0.3$, (e) $\alpha = 0.2$, (f) $\alpha = 0.1$, (g) $\alpha = 0.025$, (h) $\alpha = 0.01$. Note that the x- and y-scales are changed as α varies.

determined as the closest distance of the first ring, as can be seen in figure 3. Following this approach we obtain that in the small-κ region the frequency ω increases linearly with κ and that the small-κ behaviour of the frequency could be fitted to

$$\omega(\kappa)/\omega(0) = 4.94 + 1.44\kappa + 0.01\kappa^2$$

for $N = 9$. The previous normal-mode analysis of reference [20] for Coulomb systems showed that the spectrum exhibited three frequencies (in units of $\omega_0/\sqrt{2}$) which are independent of the number of particles: (i) $\omega = 0$: due to the uniform rotation of the system; (ii) $\omega = \sqrt{2}$: due to the centre-of-mass motion of the whole system ($\omega = \omega_0$ in real units); and (iii) $\omega = \sqrt{6}$: the breathing mode. For the present screened Coulomb system, the centre-of-mass motion is still independent of N and κ due to the generalized Kohn theorem [21] which is valid for parabolic confinement independently of the functional form

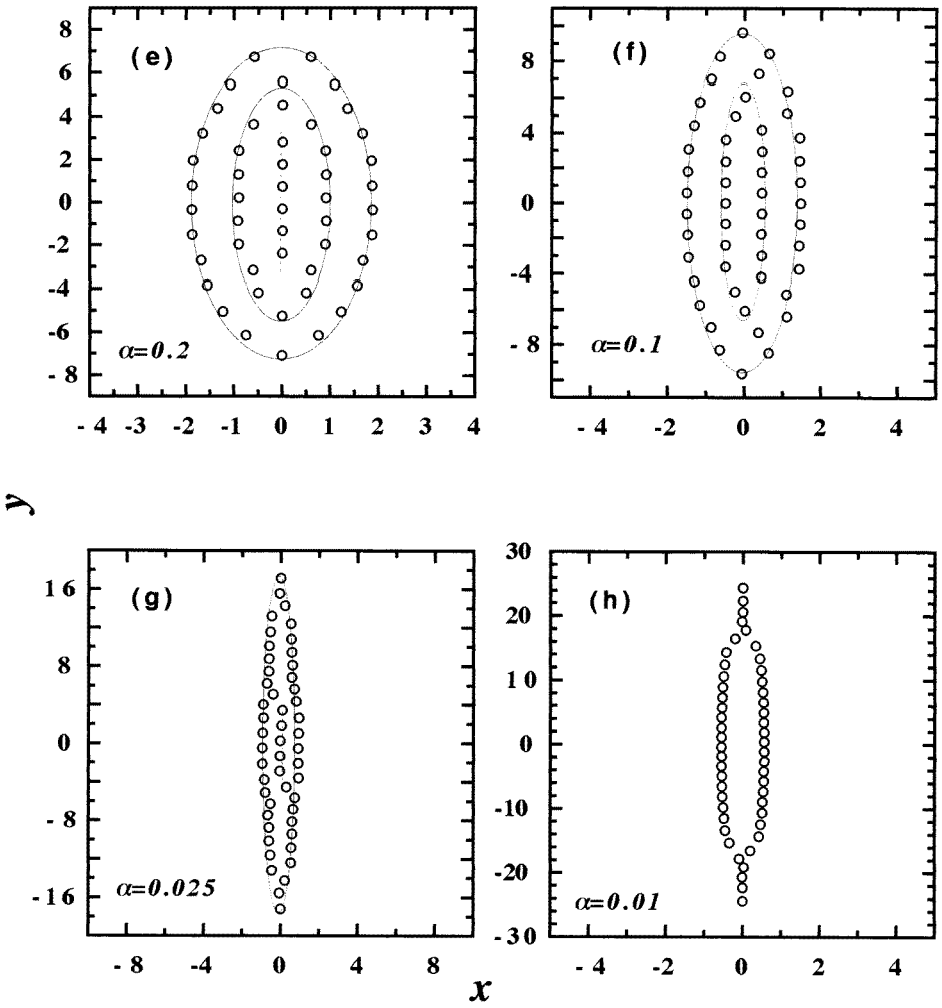

Figure 9. (Continued)

of the inter-particle potential. The frequency of the breathing mode, on the other hand, depends on κ, and for $\kappa \neq 0$ depends also on N. This is illustrated in figure 8, where we show the frequency of the breathing mode as a function of the screening constant κ for $N = 2, 3, 5, 9$.

4. Anisotropic confinement of Coulomb clusters

Next we turn our attention to the effect of the symmetry of the confinement potential on the stable-state configuration of the cluster. In order to limit the number of parameters, we consider first the Coulombic inter-particle interaction, i.e. $\kappa = 0$. In references [8] and [9], the effect of the functional form of the confinement potential, the hard wall [8] and a general r^n-potential [9], was considered. But the confinement potential had still circular symmetry. By changing α in equation (1), we can go from a circular potential

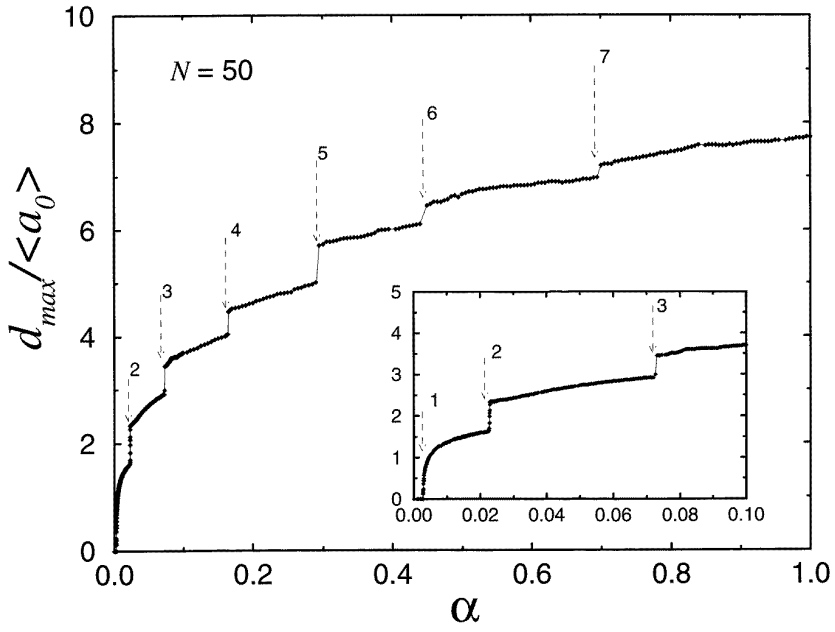

Figure 10. The maximum distance between two particles in the x-direction as a function of the anisotropy parameter in the $N = 50$ cluster. The distance is scaled with respect to the mean nearest-neighbour distance $\langle a_0 \rangle$.

($\alpha = 1$) to a 1D system ($\alpha = 0$), when the confining force along one axis is strongly reduced.

4.1. The structure of the equilibrium-state configuration

The positions of the particles for a system of $N = 50$ particles are depicted in figure 9 for different values of the anisotropy parameter: (a) $\alpha = 1.0$, (b) $\alpha = 0.7$, (c) $\alpha = 0.5$, (d) $\alpha = 0.3$, etc. Note that, for the isotropic case ($\alpha = 1$), the shell structure is recovered with the following occupation of the different rings: $(4, 10, 16, 20)$, which agrees with the one found in reference [8]. On decreasing α, this ring structure becomes deformed due to the increasingly elliptic shape of the confinement potential. For α near 1 (see figure 9(b)), there is only a continuous plastic deformation of circular to elliptical rings, which are nothing else than the equipotential lines of the confinement potential. On decreasing α further, we found that there are structural transitions in which the stable-state configuration changes in a discontinuous manner. For example, on going from $\alpha = 0.7$ (figure 9(b)) to $\alpha = 0.5$ (figure 9(c)), the inner ellipse collapses into a line and, at the same time, there is a redistribution of the particles between the different elliptical rings. Still decreasing α, the central line of particles disappears (see figure 9(d)) and the particles redistribute themselves over the three elliptical rings. This scenario repeats itself when we decrease α further. Following reference [14], we analysed these transitions in a more quantitative way by calculating the ratio $d_{\max}/\langle a_0 \rangle$ for electrons in the configuration. The maximum distance $d_{\max}$ between electrons in the x-direction is defined by the position of the last one of the three peaks of the pair-correlation function along the x-axis. This quantity is scaled with respect to $\langle a_0 \rangle$, which is the smallest distance between two particles in the cluster, and defined as the position of

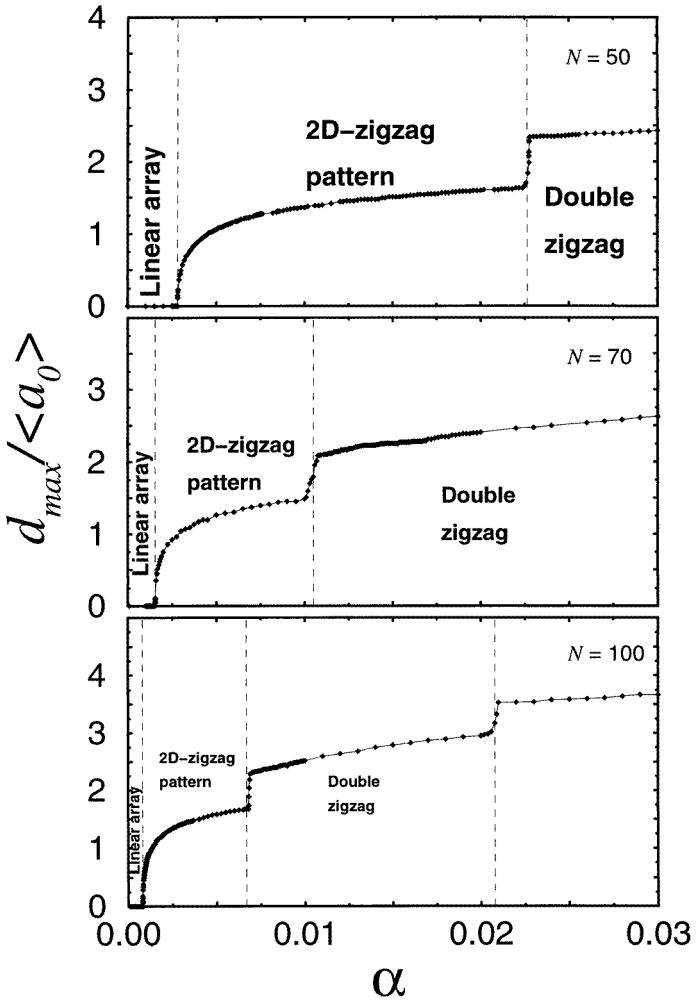

Figure 11. As figure 10, but now only the small-α region is considered for (a) $N = 50$, (b) $N = 70$, and (c) $N = 100$.

the first peak in the total pair-correlation function. The normalized distance $d_{\max}/\langle a_0 \rangle$ is plotted in figure 10, which shows clear discontinuous behaviour at seven different values of α. The differences between the different configurations are apparent from figure 10 where, as α varies, we notice, in the centre of the cluster, periodic alternations of a line of particles and particles arranged on an ellipse. With decreasing α, the width of the cluster along the x-direction decreases until we arrive at a line arrangement of particles in the y-direction for $\alpha < 0.025$. Increasing α beyond this value results in a zigzag transition for the particles in the centre of the line. This is similar to what was found in reference [19] for a ring confinement potential, but with the essential difference that in the latter case all particles take part in the zigzag transition and this transition occurs with increasing number of particles, while here it occurs with decreasing anisotropy of the confinement potential and initially only the central particles in the line take part in the zigzag transition.

The dependence of the zigzag transition on the number of particles is illustrated in

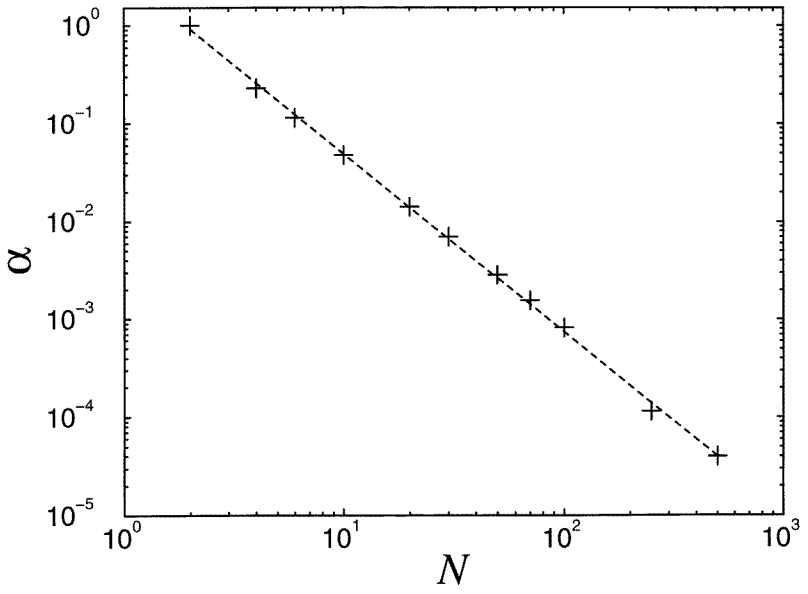

Figure 12. The value of the anisotropy parameter at which the first zigzag transition occurs as a function of the number of particles in the cluster. The symbols are the results from our simulations and the line is a power-law fit.

figure 11. Notice that with increasing N, the different transitions move towards smaller values of α, i.e. larger anisotropy, but the $d_{\max}/\langle a_0 \rangle$ value at the transitions practically does not depend on N. Furthermore, the general shape of the curves is independent of N. The position of the first zigzag transition is plotted in figure 12 as a function of the number of particles in the cluster. The decrease of α with increasing N is a consequence of a stronger potential in the y-direction. Since, on increasing N, more particles are pushed away from the $y = 0$ centre, which increases the potential energy of the system, then consequently the zigzag transition will occur for a much smaller confinement potential in the y-direction, i.e. for smaller α-values. The dashed line in figure 12 is a power-law fit to the numerically calculated values (indicated by symbols): $\alpha_{tr} = cN^{\beta}$, where we found $\beta = 1.82$ and $c = 3.23$. Note that this power-law behaviour is similar to the one found for the zigzag transition in a confined 3D ionic anisotropic system [14], but with different values for β and c.

4.2. The minimum energy of the equilibrium state

The lowest energy of the stable state per particle as a function of the anisotropy parameter is shown in figure 13 for three different cluster sizes: $N = 50, 70$, and 100. For $\alpha = 1$, we recover the results of reference [8]. Note that the energy is a smooth function of α, and no effects due to the transitions shown in figures 10 and 11 are visible. On increasing the anisotropy, the energy per particle decreases because the number of nearest neighbours decreases (see e.g. figure 9) which are responsible for the largest contribution to the interaction energy.

The energy per particle is an increasing function of the number of particles but increases less than linearly in N. The energy followed approximately an $E \sim N^{5/3}$ behaviour. The

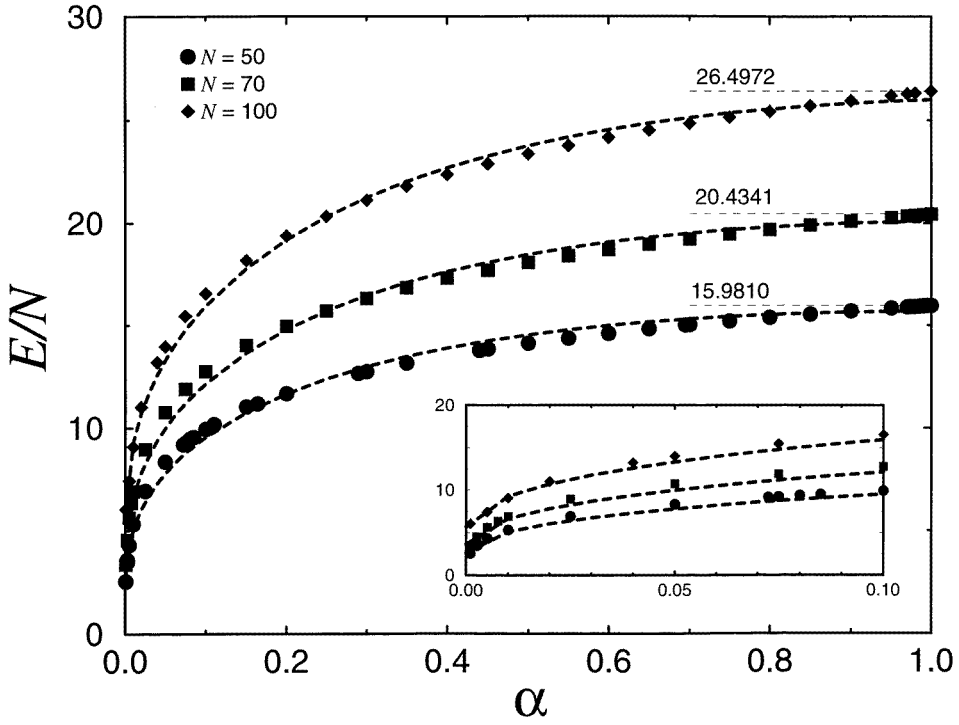

Figure 13. The lowest energy of the equilibrium configuration as a function of the anisotropy parameter for clusters with $N = 50$, 70, and 100 particles. The symbols show our results and the curves are power-law fits.

α-dependence could be well fitted (dashed curves in figure 13) to $E/N = a + b\alpha^{1/2} + c\alpha$ with $\{a = 2.64;\ b = 25.88;\ c = -12.83\}$ for $N = 50$, $\{a = 3.62;\ b = 31.85;\ c = -15.39\}$ for $N = 70$, and $\{a = 5.65;\ b = 38.22;\ c = -17.88\}$ for $N = 100$.

4.3. Dynamical properties

The normal-mode spectrum was again obtained from the peak positions in the Fourier transformed velocity auto-correlation function. The spectrum for a system of $N = 9$ particles is shown in figure 14 as a function of the anisotropy parameter. Note that for $\alpha \neq 1$, the rotational mode, which for $\alpha = 1$ has the frequency $\omega = 0$, now attains a nonzero value due to the loss of circular symmetry. Its frequency increases with decreasing α. As a consequence, the lower bound of the normal-mode spectrum increases as α decreases. The frequency of the centre of mass motion is still independent of the number of particles in the system, as was shown in reference [21], but is now different for motion along the x-direction ($\omega = \omega_0$) and for motion along the y-direction ($\omega = \sqrt{\alpha}\omega_0$). These frequencies are shown by the dashed curves in figure 14. The breathing mode which was present in the circular symmetric system and has frequency $\omega = \sqrt{3}\omega_0$ becomes a function of the anisotropy parameter α and evolves into a more complicated normal mode of the system. Note also that the maximum frequency of the spectrum deceases with decreasing α which is a consequence of the overall softening of the confinement potential and the increased extent of the system (see figure 9).

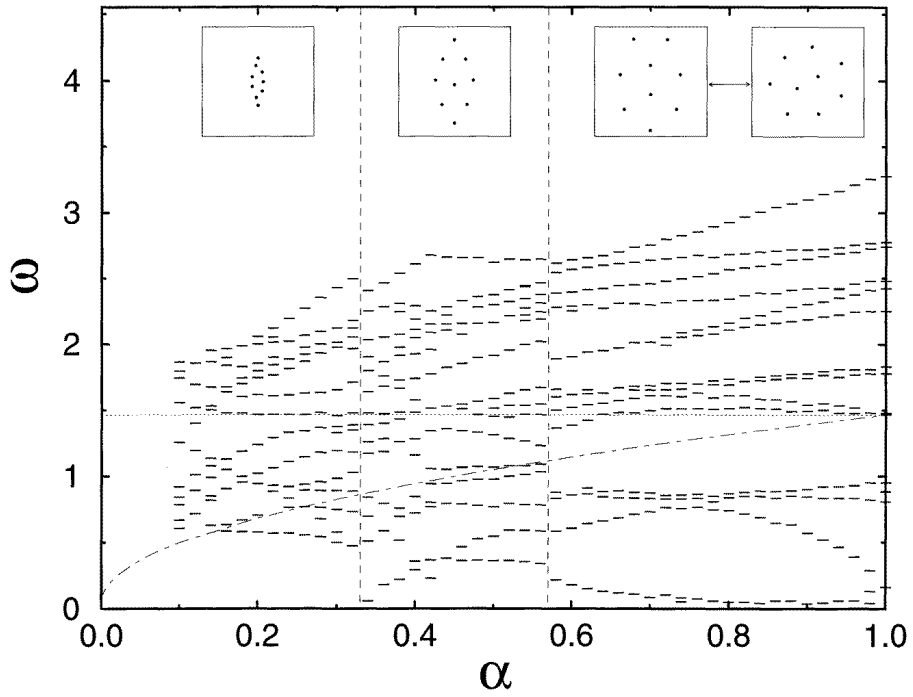

Figure 14. The mode spectrum as a function of the anisotropy parameter for a cluster of $N = 9$ particles. The vertical lines indicate the structural transitions for different configurations which are shown in the insets.

The configurations of the $N = 9$ system are given as insets in figure 14. We observe that the spectrum changes discontinuously for $\alpha = 0.33$, and 0.57, where the structure of the stable state changes abruptly. At $\alpha \approx 0.4$, a plastic deformation occurs in the cluster, but without any drastic change in the configuration. Consequently, in contrast to the behaviour of the minimum energy of the stable state, the structural transitions are reflected in the spectrum of normal modes. Thus, the normal modes are more sensitive to the exact configurations of the system than the stable-state energy.

5. Summary and conclusions

For the sake of completeness, we have also studied the influence of the screening constant of the Yukawa potential on the structural transitions driven by the anisotropic confinement. In figure 15, we depict the maximum distance between two electrons in the $N = 50$ cluster as a function of the anisotropy parameter to show the influence of the screening potential on the first transition, as displayed in figure 10. We observe a shift of the transition point to lower values of α with increasing κ. But, on increasing κ, beyond $\kappa = 5$ we do not see any significant changes in the critical value of α. This behaviour can be understood as follows. Increasing the screening brings the particles closer together and as a consequence the influence of the confinement potential on the stable-state configuration is diminished. As a result, larger anisotropies are needed, i.e. smaller α-values, in order to drive the stable-state configuration into a single line.

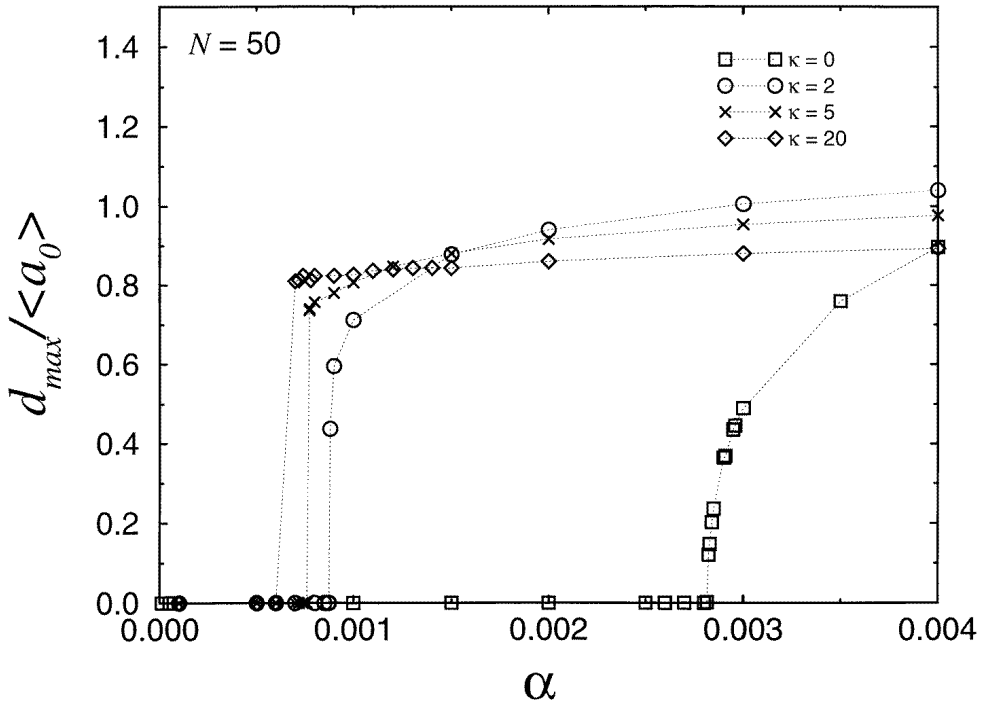

Figure 15. The maximum distance between two particles in the x-direction as a function of the anisotropy parameter around the first structural transition, as plotted in figure 10, for different values of the screening constant.

In summary, the stable-state configuration and the dynamics of a 2D classical system of charged particles confined by a harmonic oscillator potential were investigated. The dependence of the stable state on the number of particles (N), the screening of the inter-particle potential (κ), and the anisotropy (α) of the confinement potential was studied in detail. As function of α and κ, different structural transitions were found. On increasing the screening, i.e. making the inter-particle interaction potential more short ranged, the distribution of the particles over the different shells is altered and, in the limit of large screening, the particles form a Wigner lattice at the bottom of the confinement potential.

The effect of the anisotropy was investigated in detail for the case of particles interacting through a bare Coulomb potential. Making the system more anisotropic, the circular shells are deformed into ellipses and the number of shells decreases; this occurs through a number of structural phase transitions at which the inner shell collapses into a line. In the limit of extreme anisotropy of the confinement potential, a 1D configuration of particles is found.

Both α and κ strongly influence the frequency of the modes of the system. The increase of the screening allows the particles to be closer to each other which leads to a substantial increase of the normal-mode frequencies. On the other hand, increasing the anisotropy of the system contracts the spectrum into a smaller frequency region in which the bottom of the spectrum moves up in energy while the top of the spectrum moves down in energy. We found that the spectrum is a much more sensitive quantity than the minimum energy of the equilibrium configuration as regards seeing signatures of the structural transitions in the system.

Acknowledgments

This work was partially sponsored by Conselho Nacional de Desenvolvimento Científico e Tecnológico (CNPq), Fundação de Amparo à Pesquisa do Estado de São Paulo (FAPESP), and the Flemish Science Foundation (FWO). One of us (LC) is supported by Fundação Coordenação de Aperfeiçoamento de Pessoal de Nível Superior (CAPES). The final part of this work was performed when FMP was a visitor at the Universidade Federal de São Carlos.

References

[1] See, for instance,
Sikorski C and Merkt U 1989 *Phys. Rev. Lett.* **62** 2164
Weiss J, Haug R J, von Klitzing K and Ploog K 1992 *Phys. Rev.* B **46** 12 837
Ashoori R C, Stormer H L, Weiner J S, Pfeiffer L N, Pearton S J, Baldwin K W and West K W 1992 *Phys. Rev. Lett.* **68** 3088
Wagner M, Merkt U and Chaplik A V 1992 *Phys. Rev.* B **45** 1951
Matulis A and Peeters F M 1992 *J. Phys.: Condens. Matter* **6** 7751
Farinas P F, Marques G E and Studart N 1996 *J. Appl. Phys.* **79** 8475
[2] Toschek P E 1984 *New Trends in Atomic Physics (Les Houches, Session 38)* vol 1, ed G Grynberg and R Stora (Amsterdam: North-Holland) p 383
Levi B G 1988 *Phys. Today* **41** 17
Haizen M G, Gilligan J M, Berquist J C, Itano W M and Wineland D J 1992 *Phys. Rev.* A **45** 6493
[3] Rahman A and Schiffer J P 1986 *Phys. Rev. Lett.* **57** 1133
Birkl G, Kassner S and Walther H 1992 *Nature* **357** 310
Hangst J S, Nielsen J S, Poulsen O, Shi P and Schiffer J P 1995 *Phys. Rev. Lett.* **74** 4432
[4] Leiderer P 1997 *Two-dimensional Electron Systems on Helium and Other Substrates* ed E Y Andrei (Dordrecht: Kluwer)
Leiderer P 1995 *Z. Phys.* B **98** 303
Vinen W F 1995 *Z. Phys.* B **98** 299
[5] Chu J H and Lin I 1994 *Phys. Rev. Lett.* **72** 4009
Thomas H, Morfill G E, Demmel V, Goree J, Feuerbacher B and Möhlmann D 1994 *Phys. Rev. Lett.* **73** 652
Chiang C-H and Lin I 1996 *Phys. Rev. Lett.* **77** 647
[6] Pieranski P, Strzelecki L and Pansu B 1983 *Phys. Rev. Lett.* **50** 900
van Winkle D H and Murray C A 1986 *Phys. Rev.* A **34** 562
Murray C A and van Winkle D H 1987 *Phys. Rev. Lett.* **58** 1200
Murray C A and Wenk R A 1989 *Phys. Rev. Lett.* **62** 1643
Hug J E, van Swol F and Zukoski C F 1995 *Langmuir* **11** 111
Neser S, Palberg T, Bechinger C and Leiderer P 1997 *Prog. Colloid Polym. Sci.* **104** 194
Totsuji H, Kishimoto T and Totsuji C 1997 *Phys. Rev. Lett.* **78** 3113
[7] Thomson J J 1904 *Phil. Mag.* **7** 137
[8] Bedanov V M and Peeters F M 1994 *Phys. Rev.* B **49** 2667
[9] Partoens B and Peeters F M 1997 *J. Phys.: Condens. Matter* **9** 5383
[10] Schweigert V A and Peeters F M 1995 *Phys. Rev.* B **51** 7700
[11] Partoens B, Schweigert V A and Peeters F M 1997 *Phys. Rev. Lett.* **79** 3990
[12] Kremer K, Robbins M O and Crest G S 1986 *Phys. Rev. Lett.* **57** 2694
Hunter R S 1989 *Foundations of Colloid Science* vol 2 (New York: Oxford University Press)
[13] Peeters F M and Wu X G 1987 *Phys. Rev.* A **35** 3109
[14] Schiffer J P 1993 *Phys. Rev. Lett.* **70** 818
[15] Hasse R W and Schiffer J P 1990 *Ann. Phys., NY* **203** 419
[16] Bolton F and Rössler U 1993 *Superlatt. Microstruct.* **13** 139
[17] Farias G A and Peeters F M 1996 *Solid State Commun.* **100** 711
[18] Koulakov A A and Shklovskii B I 1998 *Phys. Rev.* B **57** 2352
[19] Schweigert I V, Schweigert V A and Peeters F M 1996 *Phys. Rev.* B **54** 10 827
[20] Schweigert V A and Peeters F M 1998 *J. Phys.: Condens. Matter* **10** 2417
[21] Peeters F M 1990 *Phys. Rev.* B **42** 1486